Ionic contrast across a lipid membrane for Debye length extension: towards an ultimate bioelectronics transducer

Donggeun Lee
Korea Institute of Science and Technology
Suho Lee
Korea Advanced Institute of Science and Technology
Eui-Sang Yu
Korea Institute of Science and Technology https://orcid.org/0000-0002-7833-7303
Taikjin Lee
Korea Institute of Science and Technology
Jae Hun Kim
Korea Institute of Science and Technology
Hyun Seok Song
Korea Institute of Science and Technology
Kwan Hyi Lee
Korea Institute of Science and Technology https://orcid.org/0000-0002-7891-844X
Seok Lee
Korean Institute of Science and Technology
Sang-Kook Han
Yonsei University
Myung Chul Choi
Korea Advanced Institute of Science and Technology
Yong-Sang Ryu (ysryu82@kist.re.kr)
Korea Institute of Science and Technology https://orcid.org/0000-0002-3222-4231
Chulki Kim
Korea Institute of Science and Technology https://orcid.org/0000-0002-9806-5122

Article

Keywords: field effect transistors, receptor-ligand bindings, Debye length extension

Posted Date: November 4th, 2020

DOI: https://doi.org/10.21203/rs.3.rs-96572/v1

Version of Record: A version of this preprint was published at Nature Communications on June 18th, 2021. See the published version at https://doi.org/10.1038/s41467-021-24122-8.

Abstract

Despite technological advances in biomolecule detections, evaluation of molecular interactions via potentiometric devices under ion-enriched solutions has remained a long-standing problem. To avoid severe performance degradation of bioelectronics by ionic screening effects, we cover probe surfaces of field effect transistors (FETs) with a single film of the supported lipid bilayer (SLB), and realize outstanding potentiometric signals from receptor-ligand bindings irrespective of ionic strength of bulky solutions by placing an ion-free water layer underneath the SLB. High-energy X-ray reflectometry together with the circuit analysis discovered biochemical findings that effective electrical signals dominantly originated from the sub-nanoscale conformational change of lipids in the course of receptor-ligand bindings. Beyond thorough analysis on the underlying mechanism at the molecular level, the proposed SLB-FET platform ensures the world-record level of sensitivity in molecular detection with excellent reproducibility regardless of molecular charges and environmental ionic conditions.

Introduction

Evaluation of molecular interaction is an indispensable step to unveil molecular-level of chemical processes and resultant biological functions. As an effort of understanding the mechanisms underpinning biological processes, detection of molecules or molecular interplay with counterparts have studied via surface-sensitive bioelectronics. Target-specific surface functionalization on a probe surface is an essential step to unveil molecular interactions between surface-tagged molecules and their counterparts, such as antibody–antigen complexes[1, 2], complementary single-stranded deoxyribonucleic acid[3, 4], and enzyme–substrates[5]. Via a potentiometric scheme, potential variation, arising from the adsorption/desorption of biomolecules on the probing electrodes, is effectively transduced into carrier density variation within an active current channel. Among a variety of probing transducers, field effect transistors (FETs) have demonstrated its unique strengths in cost effective mass production, and seamless integration with manufacturing processes as they monitor molecular binding kinetics occurred at the electrode-biomolecule interface[7, 8]. Despite significant potential as a molecule sensor, a signal achievement with FETs in ionic solutions at physiologic concentrations remains an ongoing challenge, mainly because of the formation of an “electrical double layer (EDL)” over the active sensing probe (Fig. 1a) [9]. Formation of the EDL originates from the fact that analytes attract counter ions from ionic-enriched environments, causing exponential decay of electrical potential with distance, termed Debye length (λ_D), for example, which is less than 1 nm in physiological conditions[10]. This screening effect clearly limits the detection of induced potential variation by the molecular interaction, thereby severely degrading the effective detection range. In addition, nonspecific binding to the probe also degrades sensor reliability by disrupting their selective sensing principles aiming target molecules. Thus, a novel strategy that can overcome the aforementioned hurdles is in high demand for unraveling the physicochemical nature of molecular interaction under ion-enriched environmental conditions.

To overcome the extremely short effective detection range for molecule sensing in ionic environmental conditions, diverse efforts have been undertaken by facilitating advanced measurement scheme and functional materials such as heterodyne detection[11], antibody fragments[12], and deformable aptamers[13], just to mention a few. Those results have certainly shed light on molecular detection in ionic solutions. However, they still have certain limitations or require enhancements. The heterodyne detection, which results in complexity of the operating circuitry, was not functioned under physiological ionic strength conditions. Antibody fragments are placed on the probe surface with random orientations, which often degrades measurement reproducibility. Although deformable aptamers resolve previous shortcomings, aptamers require additional laborious work on their specific design for individual target analytes. Along this line of thought, an ideal platform for biosensing applications is considered to, especially in physiological ionic strength conditions, be far from being established.

Here, we covered the probe surface of the FET with a single layer of a supported lipid bilayer (SLB), and realized an outstanding potentiometric transducer for the detection of receptor-ligand bindings irrespective of ionic strengths of bulky solutions by placing an ion-free water layer underneath the SLB. The potential of the SLB as a bioelectronic transducer derives from unique material properties of the SLB: i) high resistivity to nonspecific protein adsorption[15], ii) surface passivation with ion-impermeability[14], and iii) morphological preservation of receptors[16]. Integration of an electrical transducer with a biological interface lead to creation of exceptional molecular detectability in terms of sensitivity and selectivity under biologically relevant conditions, and finally offer a hint to investigate the origin of electric signals during sub-nanoscale physicochemical variation in the course of molecular bindings.

Result

Fabrication and measurement set-up

The measurement set-up for molecular detection comprises an FET and a reaction chamber placed on an extended gate (EG) (Figs. 1b and d). We fabricated FETs with an active current channel in nanoscale by facilitating conventional semiconductor fabrication techniques (Fig. 1c and Supplementary Fig. S1). The thickness ratio of the top (14 nm) and bottom (750 nm) oxide layers determines its figure of merit[17]. The top gate electrode is electrically connected to an indium tin oxide (ITO) layer working as the EG electrode (see Supplementary information 1 for details), wherein the gate potential change modulates the conductance in the FET. This allows for reliable data acquisition by eliminating any possible contamination or damage to the active channel of the FET. Furthermore, all the responses are transduced by an identical FET device, which enables direct comparison of individual signals measured with different analytes at various concentrations. To maximize the response amplitude, the back-gate voltage (V_{BG}) was adjusted to ensure the maximum slope in the top gate response curve (Supplementary Fig. S3).

Real-time monitoring of SLB coverage

SLB formation by spontaneous rupture of small unilamellar vesicles [SUV; 1 μg/mL in deionized water (DIW)] was examined using the FET (Fig. 2a). The SUV solution comprises 95% 1,2-dioleoyl-sn-glycero-3-phophocholine (DOPC) and 5% 1-oleoyl-2-[12-biotinyl (aminododecanoyl)]-sn-glycero-3-phosphoethanolamine (B-PE). Figure 2b shows the potential variation of the top gate electrode converted from the obtained current during the SLB formation (see Methods). The observed saturation after the fourth injection of the SUV is consistent with the calculation that 0.4 μg of lipids is sufficient to completely cover the SiO_2 surface of the EG (see Supplementary information 5 for details). An epifluorescence microscopy was used for the cross-validation of the SLB formation (the inset of Fig. 2b).

Figure 2c shows drain current (I_D) as a function of V_{BG} with different SLB compositions, for direct comparison with compositional variations. The graph displays a signal resulting from the SLB containing 1 mol% of negatively charged Texas Red 1,2-dihexadecanoyl-sn-glycero-3-phosphoethanolamine (TR-DHPE)[18] and shows a positive threshold voltage shift compared to the neutral SLB (DOPC 100%). Note that our SLB-FET platform demonstrates sufficient molecular sensitivity to distinguish compositional differences within the SLB. For a fluorescence recovery after photobleaching (FRAP) test, we prepared a sample with the mol% ratio of 94:5:1 of DOPC:B-PE:TR-DHPE. The bleached region was recovered to 80% level of the initial fluorescent intensity after 10 min (Fig. 2d). With the lateral diffusion property of the lipids and the SLB with this compositional ratio, two effective binding sites of a single avidin is assumed to be occupied avoiding steric hindrance[19]. The diffusion rate was calculated to be 1.43 ± 0.4 $\mu m^2/s$ with high uniformity over the SiO_2-coated EG[20, 21].

Measurements of biotin-avidin bindings and analytical models

To evaluate our SLB-FET as a biosensor operating in an ionic solution, we conducted time-lapse measurements during biotin–avidin binding. The SLB containing 5% of B-PE with 95% of DOPC was prepared on the EG surface[19]. After SLB deposition through SUV rupture in DIW, the outer buffer (OB) solution above the SLB was exchanged with 1× phosphate buffer saline (PBS) to mimic physiologic conditions. Note that the ion impermeability of the SLB preserves the ionic imbalance across the lipid membrane (Supplementary Figs. S4 and S5). Figure 3a shows a typical real-time trace obtained from sequential steps including SLB formation (markers 1 and 2), OB exchange from DIW into 1× PBS (marker

3), 800 pM-avidin injections (markers 4, 6, and 8), and 800 pM-Cholera toxin subunit B (CTxB) injections (markers 5 and 7). CTxB was applied as a negative control analyte. While CTxB injections showed no response, avidin injections led to clear top gate voltage change (ΔV_{TG} ~ 4.7 mV in the first injection) (Fig. 3b).

The real-time responses of biotin-avidin bindings at different analyte concentrations ranging from 100 pM to 100 nM are shown in Fig. 3c and summarized in Fig. 3d. To account for the obtained responses, an analytical model was suggested by combining the Langmuir isotherm model with the information of capacitively induced charges on the gate electrode of the FET. The induced voltage change ΔV_{TG} can be described as

$$\Delta V_{TG}([A]) = \frac{q_A}{C_{TG}}[B]_{\max}\frac{[A]}{[A]+K_{eq}} \qquad (1)$$

where q_A is the effective charge induced by molecular adsorption, $[B]_{\max}$ is the number of binding sites on the lipid membrane, $[A]$ represents the analyte concentration, and K_{eq} is the equilibrium constant[22]. The K_{eq} of 621.9 pM for biotin–avidin binding was determined from the fitting using Eq. (1) (solid line in orange, Fig. 3d), which is consistent with the literature[19, 23]. To determine binding parameters, a resistor-capacitor (RC) circuit model was combined with the first order Langmuir adsorption equation (see Supplementary information 7 for details). The time-dependent ΔV_{TG} is then expressed as

$$\Delta V_{TG}(t) = \begin{cases} \frac{q_A}{C_{TG}}[B]_{\max}(1-e^{-(k_1[A]+k_{-1})t}) + V_p(1-e^{-\frac{t}{\tau_1}}) & t < T \\ \frac{q_A}{C_{TG}}[B]_{\max}(1-e^{-(k_1[A]+k_{-1})t}) + V_p e^{-\frac{t}{\tau_2}} & t \geq T \end{cases} \qquad (2)$$

where k_1 and k_{-1} are the association and dissociation rate constants, respectively, V_p is the difference between the maximum sensor response ($q_A[B]_{max}/C_{TG}$) and the maximum value of $\Delta V_{TG}(t)$, and τ_1 and τ_2 are the RC time constants. The rate constants were calculated to be k_1 = 1.64 ± 0.06 × 10^7 $M^{-1}s^{-1}$ and k_{-1} =

1.02×10^{-2} s^{-1} based on fitting with the obtained value of K_{eq} (=k_{-1}/k_1) above (Fig. 3c). The response curve from the EG functionalized by biotin at an identical concentration without the SLB (circle in grey, Fig. 3d) shows a linear increase in the high concentration regime, which is attributable to the nonspecific binding[24]. In contrast, this nonspecific binding behavior was strongly suppressed by the SLB (circle in orange, Fig. 3d).

Figure 3e presents the sensor responses using different conditions for the buffer solution around the SLB. We differentiated the ionic strength of the OB with 0.01×, 0.1×, and 1× PBS, while keeping the DIW isolated underneath the SLB. Unlike the usual presumption that the sensing capability highly depends on the ionic strength of the solution, the responses to 800 pM avidin in different ionic buffer conditions were similar and within the error range of our measurements. The control experiment with 1× PBS buffer solution underneath the SLB inevitably demonstrates the importance of the ionic condition of the inner buffer (IB) in our SLB-FET sensing mechanism. In addition, $[B]_{max}$ and C_{TG} are calculated to be 1.74×10^{8} and 0.37 pF respectively in 5 mol% of the B-PE. With this, q_A is obtained to be 2.59×10^{-23} C ($\approx1.61\times10^{-4}$ electrons) from the fitting. This suggests a significant discrepancy with the previous result of about 3.43 electrons for a single avidin molecule in 1× PBS solution[25]. These counter-intuitive results exhibiting ionic strength independent FET signals led us to the following hypothesis: there could be a possible conformational change upon molecular binding, redistributing the electron density within the SLB (Fig. 3f).

Analysis on the electron density change in the SLB upon molecular bindings

To investigate the underlying sensing mechanism of our SLB-FET upon molecular binding, synchrotron X-ray reflectometry (XRR) was applied to acquire electron density profiles across the SLB (DOPC/B–PE = 95/5 in DIW) before/after avidin bindings[26]. The obtained electron density profiles from the reflectivity fits are presented in Fig. 4a (see Supplementary Fig. S9b for details). Despite the structural similarity, conformational changes to the free-standing SLB due to avidin binding are distinguishable, and are accompanied by the redistribution of electrons within the SLB. For quantitative analysis, differences in the electric field (ΔE) and chemical potential ($\Delta\psi$) were calculated using Poisson's equation (see Supplementary information 9 for details) (Figs. 4b, c, and d). The induced chemical potential difference,

$\Delta\psi$, via the avidin binding was 697 mV at the surface of the SiO_2 layer. By considering a series of potential drops along the circuit (Fig. 4e), the potential change at the top gate was calculated as 12.2 mV. This is consistent with the experimentally measured value, $q_A[B]_{max}/C_{TG}$ of 9.38 ± 3.08 mV in the FET, considering the fact that the XRR experiment was conducted under DIW conditions (EDL_{DIW} >> $EDL_{1\times PBS}$). Note that the ΔV_{TG} caused by the charges above the SLB (>55 Å in Fig. 4b) is within the range of standard deviation in the FET-measurements. To further cement our understanding, we compared the signal responses of avidin variants (neutrAvidin: pI. 6.3, streptavidin: pI. 5–6, and avidin: pI. 10.5) with different isoelectric points (pIs) under 1× PBS at the identical concentration of 800 pM (Fig. 4f). Coterminous FET responses regardless of different pIs support our finding that the majority of effective signals originate from dipole field change (*i.e.,* electron redistribution) within the SLB, not from the conjugated proteins themselves[27]. Note that this sensing mechanism in which the SLB works as a transducer allows the detection of the electroneutral analyte.

Table 1. Comparison of FET sensors for molecule detection

SLB?	Electron channel	Analyte	LOD*	Solvent type & conc.	*Refs.*
●	Si	Av*, S.Av*, N.Av*	100 *pM*	1× (100 *mM*) PBS	our work
●	CNT	S.Av	2.5 *uM*	10 *mM* PBS	(*28*)
●	CNT	S.Av	5 *uM*	1 *μM* PBS	(*29*)
●	OSC*	S.Av	10 *nM*	10 *mM* PBS	(*30*)
●	Graphene	Magainin 2	100 *pM*	10 *mM* NaF	(*27*)
●	Graphene	CTxB	12.5 *nM*	10 *mM* HEPES	(*31*)
×	Si	PSA*	75 *fg/mL*	1 *mM* PBS, 2 *mM* KCl	(*32*)
×	Si	Thrombin	330 *pM*	Acetate buffer	(*33*)
×	Si	PSA	150 *fM*	100 *μM* PBS, 100 *μM* KCl	(*34*)
×	Si	cTnT*	1 *fg/mL*	100 *μM* PBS	(*35*)
×	Si	PSA	1 *pg/mL*	1 *μM* PBS, 2 *μM* KCl	(*36*)

*LOD: limit of detection, Av: Avidin, S.Av: Streptavidin, N.Av: NeutrAvidin, OSC: Organic semiconductor, PSA: Phostate Specific Antigen, cTnT: Cardiac troponin T

Discussion

Most hitherto electrical sensing of molecules required buffer dilution to weaken the ionic strength of solutions. However, the structural integrity and molecular activity of target analytes are not guaranteed in such attenuated ionic environments. Previous experiments with the SLB over probing materials showed inevitable loss of sensitivity due to the screening effect by ion accumulation between the probing surface and SLB. Meanwhile, by placing DIW underneath the SLB, we successively traced potentiometric change by the SLB formation (Fig. 2b), as well as protein bindings above the SLB to the “world’s lowest level of the limit of detection (LOD)” in physiologic conditions of 1 × PBS with the SLB (Table 1). The exceptional capabilities of this SLB-FET system are attributable to the following: i) directional alignment of receptors, ii) defect-free coverage of the SLB, and iii) ion-impermeability of the SLB. Note that the combination of all the ingredients described above resulted in the extension of the effective detection range (= Debye length extension) via a vertical shift of stern- and diffusive-layers (Fig. 4d). X-ray reflectometry and the corresponding equivalent circuit analysis clearly explained the origin of the obtained electrical responses and their signal transfer mechanism via sub-nanoscale conformational change of lipids during binding events, which were independent from the ionic strengths of the outer buffer solution and even the effective charge states of the bound molecules (Figs. 3e and 4f). In particular, striking FET responses with coterminous amplitudes upon protein bindings with distinct pIs obviously support our findings on the sensing mechanism. To the best of our knowledge, our SLB-FET platform presents the first experimental observation of SLB conformation changes via molecular binding events with an in-vitro electrical detector, which has been long proposed as a theory but was never experimentally validated. The results obviously demonstrate that dominant electric signal arises from the dipole field variation of the underlying SLB membrane during protein bindings. This opens up an opportunity to analyse the physicochemical modulation of lipids at the molecular level, ruling out any possible contribution of the effective charge of target proteins in the signal transducing mechanism. By resolving the chronic concern of molecular detection in physiologically relevant conditions, our SLB-FET platform and resultant exceptional performances can be extended to identify essential roles of membrane-related pathogenic proteins, and stages/factors of diseases and apoptosis of cells that experiences lipid membrane rupture processes. This has wide ranging implications for conditions such as neurodegenerative disorders, including Alzheimer’s and Parkinson’s diseases[37, 38], virus-cell membrane interaction[39, 40], and the impact of micro-particles on the human respiratory system[41].

Methods

Fully depleted silicon-on-insulator device fabrication process: Conventional fabrication processes were conducted to construct FET devices, known as Si-nanoribbons[22] (Supplementary Fig. S1). SIMOX-SOI wafers (100 nm thick top-Si, Shinetsu) were used to enable top and bottom gating with high precision. In

step 1, we selectively etched the top-Si layer using a reactive ion etching (RIE) process to define the active current channel (5 μm long and 30 μm wide) in the FET. A 15-nm-thick oxide layer was formed over the entire top-Si surface using a dry oxidation process (step 2), and confirmed by transmission electron microscope (TEM, Tecnai F20 G2, FEI). For the top gate (TG) electrode, a 200-nm-thick polysilicon (poly-Si) film was deposited, followed by selective etching of the poly-Si and SiO_2 layers (steps 3 and 4). To minimize the Schottky barrier in metal contacts, arsenic (As) implantation (step 5) followed by annealing (step 6, 850°C for 30 sec) was performed. Then, Ti/TiN/Al/TiN (50/50/250/50 nm) layers were selectively etched using the RIE process, providing soldering pads (steps 7 and 8). Finally, we encapsulated the fabricated devices and mounted them on a printed circuit board with a pin-type interface.

Faraday shielding box and EG connections: The EG with the reaction chamber was placed in a metallic box for noise shielding. We applied the source and back gate bias voltages (V_S and V_{BG}) with DC voltage sources (GS210, Yokogawa, Japan) with high precision and measured the drain current (I_D) with a digital multimeter (34410A, Agilent, USA). The EG was electrically wired to the TG and terminated with an Ag/AgCl reference electrode (LF-2, Innovative Instruments, Inc., USA) (Supplementary Fig. S2).

Vesicle preparation and SLB formation: The 1,2-dioleoyl-sn-glycero-3-phophocholine (DOPC: base lipid of the SLB) and 1-oleoyl-2-(12-biotinyl(aminododecanoyl))-sn-glycero-3-phosphoethanolamine (B-PE) were purchased from Avanti Polar Lipids Inc. Avidin variants (avidin, streptavidin, and neutrAvidin) and various concentration of PBS solutions were purchased from Thermo Fisher Scientific. The SLB membrane consists of 95 mol% DOPC and 5% B-PE (receptor of avidin-variants). For vesicle preparation, we used the rapid solvent exchange method to evaporate chloroform and hydrate with buffer solution [deionized water (DIW) or 1× PBS] simultaneously[20]. After that, the prepared vesicle solutions were extruded 20 times through 50-nm-diameter pores (PC membrane, Avanti Polar Lipids Inc., USA) to prepare uniformly sized, small unilamellar vesicles (SUV; 0.1 mg/mL). The 50-nm-diameter SUVs spontaneously rupture on a hydrophilic SiO_2 surface and form a uniform and defect-free SLB patch on the SiO_2 surface of the EG[42, 43]. For negative controls for biotin–avidin binding, Cholera toxin subunit B proteins (CTxB, Invitrogen, USA) specifically bound to ganglioside GM1 lipids were used.

Measurement setup for X-ray reflectivity (XRR): Synchrotron XRR measurement was carried out using the beamline 5A, MS-XRS (16.2 keV) in the Pohang Accelerator Laboratory (PAL) with a customized liquid cell. The aluminum liquid cell has Kepton sealed windows, which are transparent to synchrotron X-ray wavelength, allowing X-ray to be reflected from the surface of the sample while maintaining an aqueous environment inside (Supplementary Fig. S6). The cross-sectional beam size of incident X-ray was 500 × 400 μm^2, which is large enough to ensure the averaging effect[44]. The SLB (DOPC:B-PE = 95:5) in the DIW

was formed via the vesicle fusion method on the 300 nm-thick SiO_2-coated Si wafer and annealed at 40°C for 30 min. We injected 800 pM-avidin solution to the SLB and waited for another 30 min to reach equilibrium in the biotin–avidin reaction. After washing to remove protein residues, the wafer was mounted in the liquid cell (Supplementary Fig. S6), which is filled with DIW before the XRR measurement.

Electron density profile in the SLB obtained from X-ray reflectivity measurement: We used the slab model based on Parratt's method[45] (fig. S9) combined with a genetic algorithm to calculate reflectivity. We modeled the SLB with five slabs: two lipid head groups, two lipid tail layers, and a single empty space between each leaflet. For avidin adsorption, four additional slabs were used: three layers of protein and a single layer of DIW between the avidin and the bilayer surfaces. The roughness between each slab was assumed to be 3 Å. Unlike the conventional SLB electron density fitting in which the symmetric electron density profile is assumed, we supposed an asymmetric structure considering that the lipid head group and tail layer in the upper leaflet and bottom leaflet can have different electron densities via avidin adsorption.

Declarations

Acknowledgments

This work was supported by KIST Institutional Programs (No. 2E30520, 2E30140, and 2E30506) and the National Research Foundation of Korea (NRF) grant funded by the Korea government (MSIT) (No.2020R1A2C2005486 and No. 2018R1A2B3001690).

Author contributions

D.L., Y.-S.R., and C.K. designed the experiments, analyzed the data, and prepared the initial draft of the manuscript. D.L. fabricated FET devices and performed SLB-FET measurements. D.L., S.L., and M.C.C. conducted XRR experiments and analysis. E.-S.Y. obtained the fluorescence microscopy images and performed the FRAP experiment. E.-S.Y., H.S.S., J.H.K., and K.H.L. prepared SLBs and test analytes and provided technical assistance in handling samples. S.L., T.L., and S.-K.H. conducted electrical signal data analysis. All authors agreed on the final content.

Competing interests

Authors declare no competing interests.

References

1. J. T. Mabeck, G. G. Malliaras, Chemical and biological sensors based on organic thin-film transistors. *Anal. Bioanal. Chem.* **384**, 343–353 (2006).
2. M. J. Schoning, A. Poghossian, Recent advances in biologically sensitive field-effect transistors (BioFETs). *Analyst* **127**, 1137–1151 (2002).
3. L. A. Thompson, J. Kowalik, M. Josowicz, J. Janata, Label-free DNA hybridization probe based on a conducting polymer. *J. Am. Chem. Soc.* **125**, 324–325 (2003).
4. Y. L. Bunimovich et al., Quantitative real-time measurements of DNA hybridization with alkylated nonoxidized silicon nanowires in electrolyte solution. *J. Am. Chem. Soc.* **128**, 16323–16331 (2006).
5. Y. W. Jiang, B. Z. Tian, Inorganic semiconductor biointerfaces. *Nat. Rev. Mater.* **3**, 473–490 (2018).
6. T. Ji et al., Detection of COVID-19: A review of the current literature and future perspectives. *Biosens. Bioelectron.* **166**, 112455 (2020).
7. J. K. Park, W. J. Cho, Development of high-performance fully depleted silicon-on-insulator based extended-gate field-effect transistor using the parasitic bipolar junction transistor effect. *Appl. Phys. Lett.* **101**, 133703 (2012).
8. M. J. Spijkman et al., Dual-gate thin-film transistors, integrated circuits and sensors. *Adv. Mater.* **23**, 3231–3242 (2011).
9. W. Huang, A. K. Diallo, J. L. Dailey, K. Besar, H. E. Katz, Electrochemical processes and mechanistic aspects of field-effect sensors for biomolecules. *J. Mater. Chem. C* **3**, 6445–6470 (2015).
10. N. Gao et al., Specific detection of biomolecules in physiological solutions using graphene transistor biosensors. *Proc. Natl. Acad. Sci. U. S. A.* **113**, 14633–14638 (2016).
11. G. S. Kulkarni, K. Reddy, Z. H. Zhong, X. D. Fan, Graphene nanoelectronic heterodyne sensor for rapid and sensitive vapour detection. *Nat. Commun.* **5**, 4376 (2014).
12. R. Elnathan et al., Biorecognition layer engineering: overcoming screening limitations of nanowire-based FET devices. *Nano Lett.* **12**, 5245 (2012).
13. N. Nakatsuka et al., Aptamer-field-effect transistors overcome Debye length limitations for small-molecule sensing. *Science* **362**, 319–324 (2018).
14. J. del Castillo, A. Rodriguez, C. A. Romero, V. Sanchez, Lipid films as transducers for detection of antigen-antibody and enzyme-substrate reactions. *Science* **153**, 185–188 (1966).
15. S. R. Tabaei, W. B. Ng, S. J. Cho, N. J. Cho, Controlling the formation of phospholipid monolayer, bilayer, and intact vesicle layer on graphene. *ACS Appl. Mater. Interfaces* **8**, 11875–11880 (2016).
16. S. Poyry, I. Vattulainen, Role of charged lipids in membrane structures - Insight given by simulations. *Biochim. Biophys. Acta* **1858**, 2322–2333 (2016).
17. M. J. Spijkman et al., Beyond the Nernst-limit with dual-gate ZnO ion-sensitive field-effect transistors. *Appl. Phys. Lett.* **98**, 043502 (2011).
18. X. J. Han *et al.*, Manipulation and charge determination of proteins in photopatterned solid supported bilayers. *Integr. Biol.* **1**, 205–211 (2009).

19. Z. Liu et al., Specific binding of avidin to biotin-containing lipid lamella surfaces studied with monolayers and liposomes. *Eur. Biophysics J.* **24**, 31–38 (1995).
20. Y. S. Ryu *et al.*, Reconstituting ring-rafts in bud-mimicking topography of model membranes. *Nat. Commun.* **5**, 4507 (2014).
21. Y. S. Ryu *et al.*, Lipid membrane deformation accompanied by disk-to-ring shape transition of cholesterol-rich domains. *J. Am. Chem. Soc.* **137**, 8692–8695 (2015).
22. X. Duan et al., Quantification of the affinities and kinetics of protein interactions using silicon nanowire biosensors. *Nat. Nanotechnol.* **7**, 401–407 (2012).
23. R. A. Kohanski, M. D. Lane, Monovalent avidin affinity columns. *Methods Enzymol.* **184**, 194–200 (1990).
24. L. Maletinska et al., Human glioblastoma cell lines: Levels of low-density lipoprotein receptor and low-density lipoprotein receptor-related protein. *Cancer Res.* **60**, 2300–2303 (2000).
25. S. Hideshima, T. Nakamura, S. Kuroiwa, T. Osaka, Relation between effective charge numbers and signals caused by protein adsorption on field effect transistor detection. *ECS Trans.* **35**, 121–124 (2011).
26. M. R. Horton, C. Reich, A. P. Gast, J. O. Radler, B. Nickel, Structure and dynamics of crystalline protein layers bound to supported lipid bilayers. *Langmuir* **23**, 6263–6269 (2007).
27. P. K. Ang et al., A Bioelectronic platform using a graphene-lipid bilayer interface. *ACS Nano* **4**, 7387–7394 (2010).
28. A. Star, J. C. P. Gabriel, K. Bradley, G. Gruner, Electronic detection of specific protein binding using nanotube FET devices. *Nano Lett.* **3**, 459–463 (2003).
29. X. J. Zhou, J. M. Moran-Mirabal, H. G. Craighead, P. L. McEuen, Supported lipid bilayer/carbon nanotube hybrids. *Nat. Nanotechnol.* **2**, 185–190 (2007).
30. M. Magliulo *et al.*, Electrolyte-gated organic field-effect transistor sensors based on supported biotinylated phospholipid bilayer. *Adv. Mater.* **25**, 2090–2094 (2013).
31. C. J. Kuo *et al.*, Lipid-modified graphene-transistor biosensor for monitoring amyloid-beta aggregation. *ACS Appl. Mater. Inter.* **10**, 12311–12316 (2018).
32. G. F. Zheng, F. Patolsky, Y. Cui, W. U. Wang, C. M. Lieber, Multiplexed electrical detection of cancer markers with nanowire sensor arrays. *Nat. Biotechnol.* **23**, 1294–1301 (2005).
33. K. S. Kim, H. S. Lee, J. A. Yang, M. H. Jo, S. K. Hahn, The fabrication, characterization and application of aptamer-functionalized Si-nanowire FET biosensors. *Nanotechnology* **20**, 235501 (2009).
34. G. F. Zheng, X. P. A. Gao, C. M. Lieber, Frequency domain detection of biomolecules using silicon nanowire biosensors. *Nano Lett.* **10**, 3179–3183 (2010).
35. J. H. Chua, R. E. Chee, A. Agarwal, S. M. Wong, G. J. Zhang, Label-free electrical detection of cardiac biomarker with complementary metal-oxide semiconductor-compatible silicon nanowire sensor arrays. *Anal. Chem.* **81**, 6266–6271 (2009).

36. A. Kim *et al.*, Ultrasensitive, label-free, and real-time immunodetection using silicon field-effect transistors. *Appl. Phys. Lett.* **91**, 103901 (2007)
37. C. Fabiani, S. S. Antollini, Alzheimer's disease as a membrane disorder: spatial cross-talk among beta-amyloid peptides, nicotinic acetylcholine receptors and lipid rafts. *Front. Cell Neurosci.* **13**, 309 (2019).
38. S. H. Shahmoradian et al., Lewy pathology in Parkinson's disease consists of crowded organelles and lipid membranes. *Nat. Neurosci.* **22**, 1099–1109 (2019).
39. L. G. M. Basso, E. F. Vicente, E. Crusca, E. M. Cilli, A. J. Costa, SARS-CoV fusion peptides induce membrane surface ordering and curvature. *Sci. Rep.* **6**, 37131 (2016).
40. K. Stadler et al., SARS - Beginning to understand a new virus. *Nat. Rev. Microbiol.* **1**, 209–218 (2003).
41. Y. F. Xing, Y. H. Xu, M. H. Shi, Y. X. Lian, The impact of PM2.5 on the human respiratory system. *J. Thorac. Dis.* **8**, E69-E74 (2016).
42. Y. S. Ryu *et al.*, Continuity of monolayer-bilayer junctions for localization of lipid raft microdomains in model membranes. *Sci. Rep.* **6**, 26823 (2016).
43. J. M. Baek, Y. S. Ryu, Surface sensitive analysis device using model membrane and challenges for biosensor-chip. *Biochip J.* **14**, 110–123 (2020).
44. S. Lee, D. W. Jeong, M. C. Choi, Vertical order of DPPC multilayer enhanced by cholesterol-induced ripple-to-liquid ordered (LO) phase transition: Synchrotron X-ray reflectivity study. *Curr. Appl. Phys.* **17**, 392–397 (2017).
45. L. G. Parratt, Surface studies of solids by total reflection of X-rays. *Phys. Rev.* 95, 359–369 (1954)

Figures

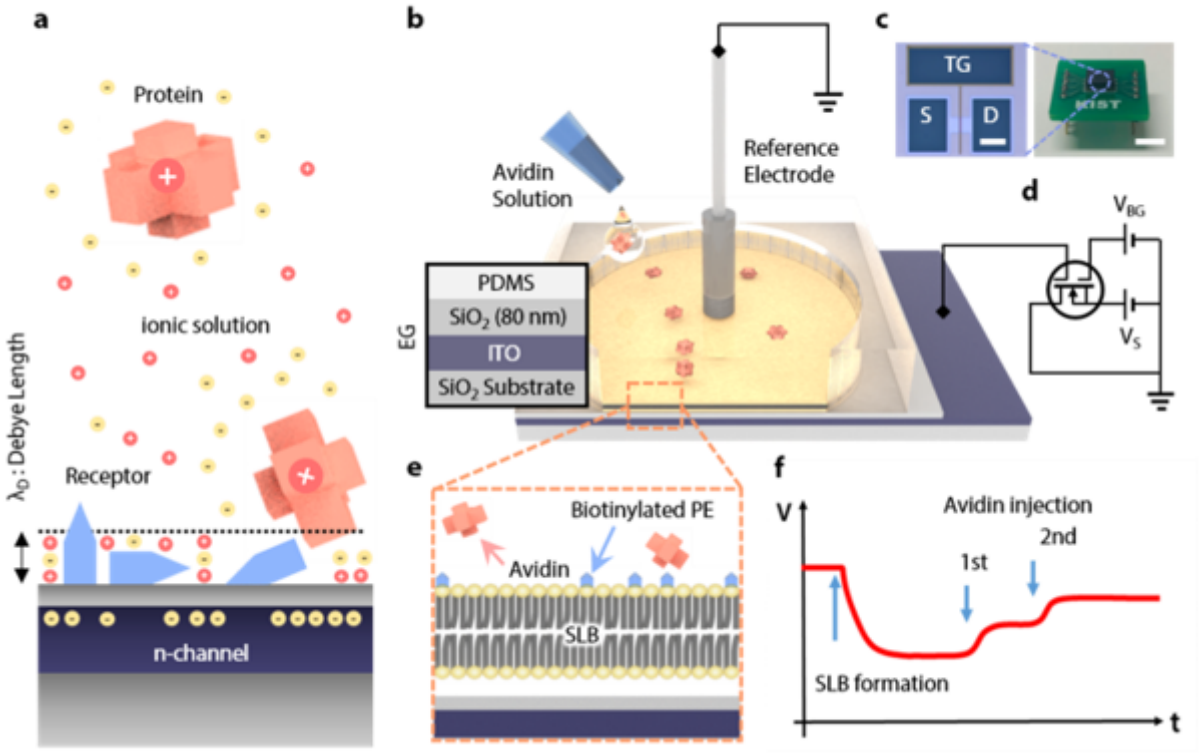

Figure 1

Electrical sensing in ionic environments and schematic of the SLB-assisted FET measurement set-up. a, Challenges to potentiometric measurement schemes for molecular detection on an FET under ionic environment: formation of the EDL, non-specific binding, and randomly oriented receptors. b, Schematic representation of a reaction chamber on the EG. (left) Layer-by-layer configuration of the EG. c, Optical images of the FET (left) and a packaged device (right) (scale bars= 100 μm and 5 mm, respectively) d, Schematic representation of measurement set-up. e, Cross-sectional illustration of the SLB on the EG surface. f, Proof-of-concept for real-time detection during biotin–avidin binding.

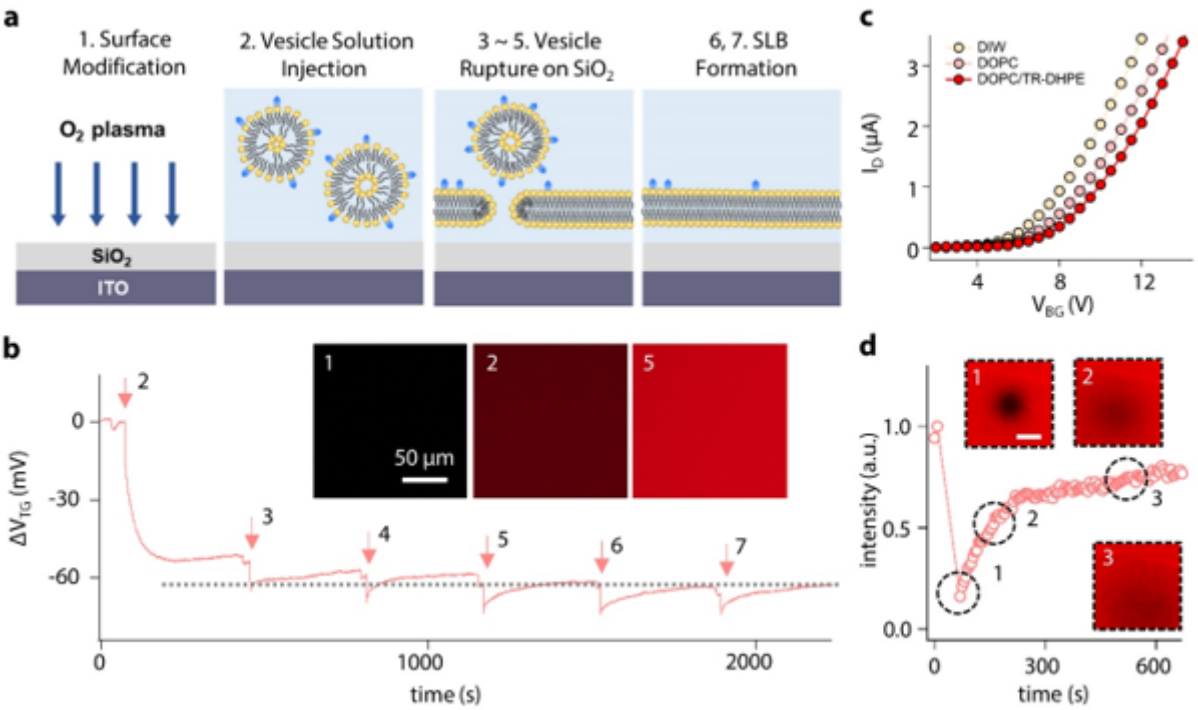

Figure 2

SLB formation and its time-dependent measurement. a, Schematic illustration of SLB formation. b, Real-time tracing during an SUV rupture process. Insets show fluorescent images of the EG after SLB formation at different vesicle concentrations; (marker 1) after O2 plasma treatment, (marker 2) at 1 μg/mL, and (marker 6) at 5 μg/mL. c, ID-VBG curves with different ingredients in the SLB. d, Time-dependent FRAP measurement. The scale bar in the inset is 50 μm.

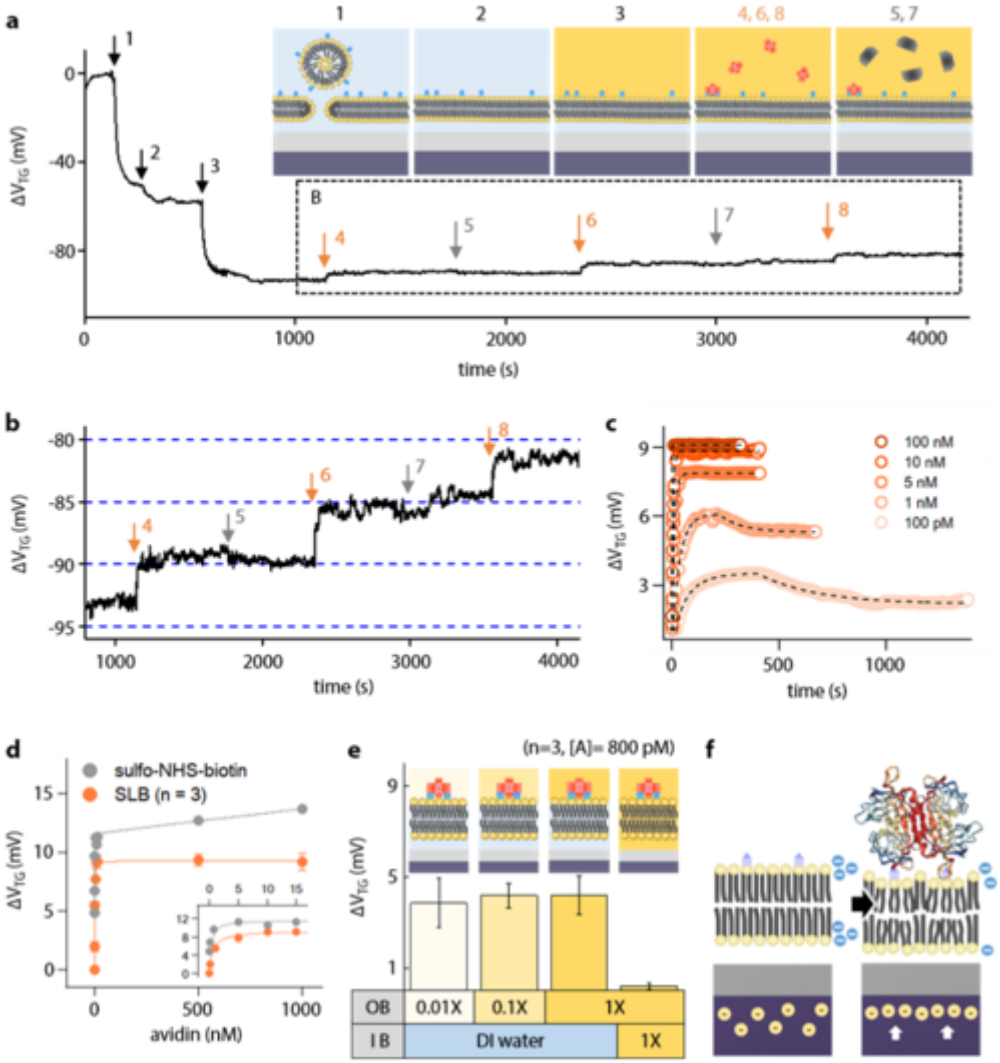

Figure 3

Measurements of biotin–avidin bindings using SLB-FET. a, Real-time measurement for SLB formation and sequential molecular bindings. The inset illustrates different measurement stages. b, Enlarged graph in Fig. 3a showing binding selectivity to avidin. c, Real-time traces (circle) from biotin–avidin binding at different concentrations. Dashed lines represent fits by an analytical model. d, Response amplitudes as a function of avidin concentration in the presence (orange)/absence (grey) of the SLB. e, Sensor responses to 800 pM-avidin injection in different ionic conditions around the SLB. f, Illustration of redistribution of electron density induced by ligand–receptor bindings.

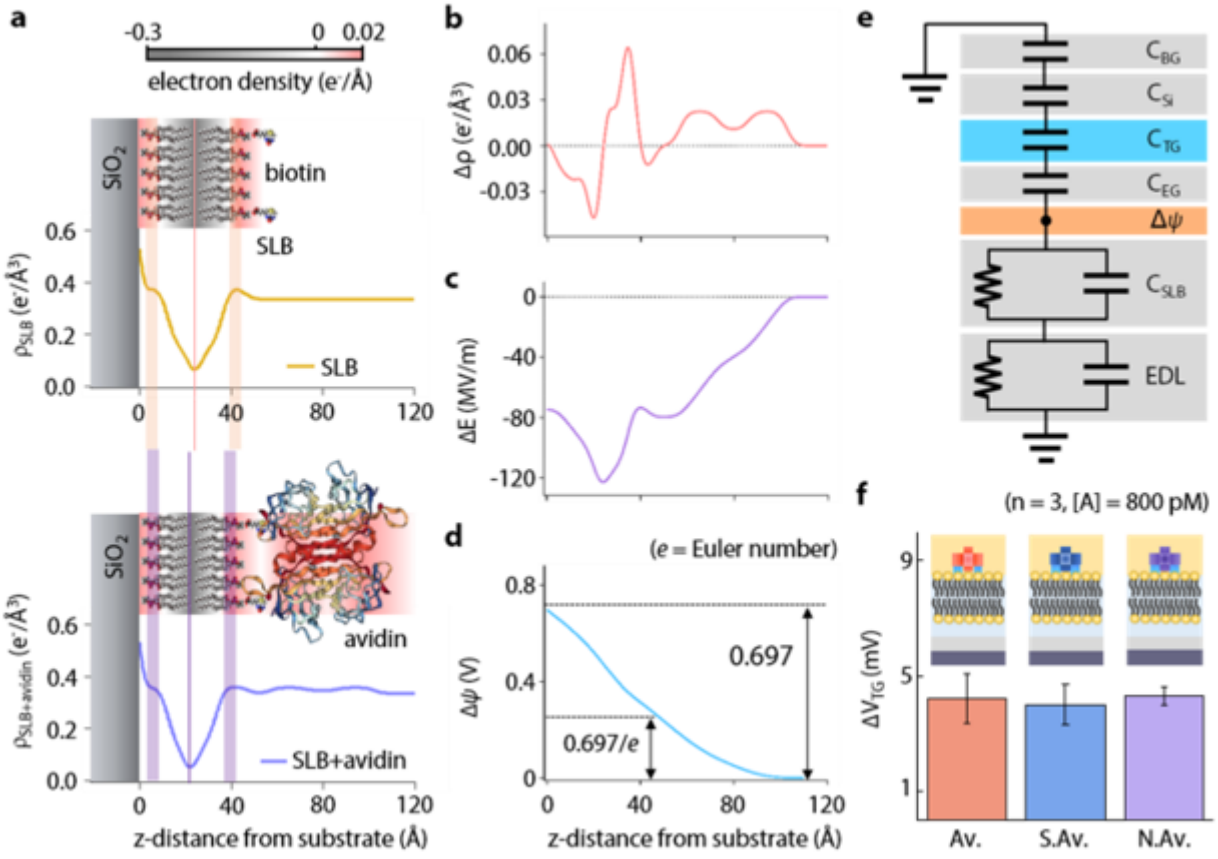

Figure 4

Redistribution of the electron density in the SLB upon biotin–avidin bindings. a, Electron density profiles before and after biotin–avidin bindings. b, Electron density difference (Δρ = ρSLB + avidin - ρSLB). c, Electric field change. d, Chemical potential difference upon biotin–avidin binding. e, Simplified electric circuit model for the measurement set-up. Potential change (Δψ) will be divided into the RC components in series. f, Sensor responses to different analytes at identical concentrations. (Av.: Avidin, S.Av.: streptavidin, and N.Av.: neutrAvidin)

Supplementary Files

This is a list of supplementary files associated with this preprint. Click to download.

- SISLBFETNC.docx